ESTIMATING TYPICAL FOUR-SEASON THERMAL DISTRIBUTION AND SELF-ADAPTIVE GRADIENT BASED THRESHOLDING PARAMETERS OVER COAL FIRE AREAS IN CHINA USING ASTER AND LDCM TIRS -A CASE STUDY IN THE WUDA COAL FIELD, CHINA

Xiaomin Du
Daiyong Cao
Guang Yang
College of Geosciences and Survey Engineering,
China University of Mining and Technology, Beijing, 100083, P. R. China
duxiaomin@gmail.com
cdy@cumtb.edu.cn
yg0817@163.com

Sergio Bernardes,
Center for Geospatial Research, Department of Geography,
The University of Georgia, Athens, GA. 30602, USA
sbernard@uga.edu

Zhipeng Li,
College of Resource and Environment,
Graduate University of Chinese Academy of Sciences, Beijing, 100049, P. R. China
lizhipeng428@gmail.com

Feng Li
Institute of Disaster Prevention, Sanhe Hebei, 101601, P. R. China
lif1223@aliyun.com

ABSTRACT

Coal fire results in significant environmental impacts and coal losses in many countries, including the United States, India, and China. Multiple fire detection methods have been proposed. Many of these rely on thermal infrared (TIR) imagery. This study results from previous research on TIR, including our development of a self-adaptive gradient based thresholding method for coal fire delineation. We used field measurements and images acquired by the ASTER sensor onboard NASA's Terra satellite and the TIRS onboard Landsat 8 to derive calibration parameters for a threshold estimation algorithm considering different solar radiation intensities, which impact radiance estimations from coal fire. We designed a simultaneous ASTER-field measurement plan in the Wuda coal field (China) and scheduled image collection for four periods, including the winter and the summer solstices (least and most intense solar radiation periods). Collection also included the vernal/autumnal equinoxes. Land surface temperature (LST) was collected before and after each satellite overpass in planned intense sampling block areas. LST field samples were integrated into 90-100 m TIR pixels. Data were combined with coal fire boundaries collected in the field and were used to validate the coal fires retrieved from four calibrated image by our temperature retrieving method, and the gradient-based threshold method. Results are a series of adjustment parameters for the fire detection method for four typical seasons. Correction parameters estimated by our method at the Wuda coal field can be extended to other fire areas lacking detailed studies, thus supporting surface temperature retrieval and underground coal fire delineation.

KEYWORDS: Thermal Infrared Remote Sensing, Coal Seam Spontaneous Combustion, Land Surface Temperature Retrieval, Digital Image Processing, Solar Radiation

INTRODUCTION

This work considers coal fire areas as burning areas caused by the spontaneous combustion in coal seam and coal waste piles. It is widely reported that coal fires result in considerable impacts to the environment, including greenhouse gas (GHG) and noxious gas emissions (Prakash, 2011; Chatterjee, 2006; Zhang, 2008, Jiang, 2011).

Detection of coal fire is an important prerequisite for the estimation for major GHG emissions and coal resource loss. Due to the heat emitted by these fires, land surface thermal anomalies associated with the coal field can be detected by thermal infrared images.

Thermal infrared remote sensing methods to detect forest fires are well studied. However, underground coal fire detection brings additional challenges, when compared to the widely applied detection of forest fires (Kuenzer, 2007a). Difficulties associated with this delineation result from the coarser pixels for thermal sensors (ASTER 90 meters, TIRS 100 meters), which limits the sensitivity of the system to fires. As a result, small fire areas and fire cracks (scale less than one pixel) are undetectable or have low radiative values in a pixel because of the sub-pixel effect. In addition, an effective and validated fire differentiation algorithm is needed, which should segment thermal anomalies by a threshold or select fire pixels in combination with the adjacent pixels in the TIR images. Further challenges include solar irradiation during daytime, resulting in this radiation signal contributing to the thermal infrared radiation caused by the coal fire. Nighttime images are ideal for coal fire detection, but these images are not always available for the ASTER sensor. The TIRS sensor onboard the Landsat Data Continuity Mission (LDCM) provides full coverage data availability, expanding the possibilities for thermal studies from orbital platforms.

The elimination of solar radiation affects is a major issue for coal fire detection based on daytime TIR images. In this regard, we attempted to reduce solar irradiation effects by removing the thermal component from land surface radiance. The work considered simulations of short wave radiation intensity from the sun on the spring/fall equinoxes and summer/winter solstices for four typical seasons. Radiation intensities for these four seasons were then converted into relative temperature increments at surface level. The calculated temperature increments were used to adjust bright temperatures.

The coal fire pixels selection mechanism in this study is segmentation with a self-adaptive thresholding method. Coal fire areas segmented by this method were validated by field measurements. Differences were observed for the values associated with coal fires retrieved from the original daytime images and from the solar radiation corrected images. This work compares the mapped anomalies for these different images sources.

GEOGRAPHICAL AND GEOLOGICAL OVERVIEW

The study area comprises the Wuda coalfield, situated the Inner Mongolia, China. This coal field is an asymmetric syncline basin with flat west wing and relative steeper east wing (Peng, 1995), the altitude is between 1046 m to 1401 m (based on the ASTER elevation product for September 26, 2013). The DEM data and our field survey in 2013 revealed the surface in this area is mountainous, rugged. The surface was deeply excavated by the opencast mining and is covered by coal waste and massive excavated sand rocks. As a result of this uneven surface, land surface temperature increases by solar radiation distribute unevenly.

The area of study has a high variety of land cover classes. Vegetation cover is relatively low (almost bare ground) even in the rainy season. Values of NDVI in this coal field indicate reduced vegetation (mean = -0.1299, max = 0.2509, and standard deviation = 0.0202), based on ASTER NIRV data acquired on June 22nd (summer solstice). The strata in the Wuda coalfield are typical Carbonic-Permian coal basin, consisting mainly of Taiyuan and Shanxi formations. There are six stable, widely distributed, and minable coal seams and 10-12 minable thin coal seams. The field includes a dominated 9 km length over-thrust fault. The fissures are widely distributed, E-W direction tectonic lines formed from Mesozoic Yanshan movement cut off the N-S direction construction lines caused by Cenozoic Himalayan orogeny (Peng, 1995; Zhang, 2008).

The coal fire area has changed significantly in the last decade, and our previous research has estimated an average burning area of 155.60 hectares. It is reported that yearly losses in coal resources in the area amount to 200,000 tons (Kuenzer, 2007b).

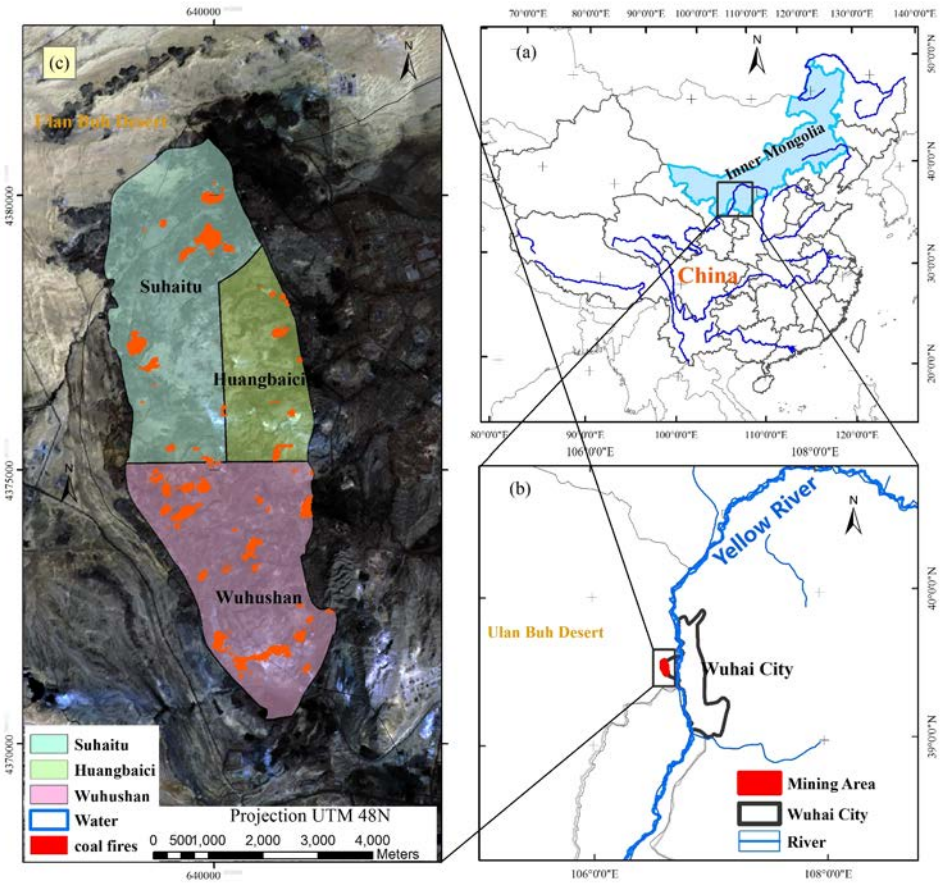

Figure 1. Location of study area, the Wuda coal field. (a) study area in China; (b) study area in Inner Mongolia; (c) coal fires area of Wuda, the "ear shaped" syncline, consists of three coal mines in the study area. The coal fires (red polygons) depict thermal anomalies for Dec 23, 2012, 03:38 am UTC (local time 10:38 am).

DATA DESCRIPTION

This work used data from two orbital imaging acquisition sensors. The ASTER (Advanced Spaceborne Thermal Emission and Reflection Radiometer) sensor onboard the Terra satellite has nine bands in two spectral regions: visible and near-infrared (VNIR) (bands 1–3) with 15-m resolution, and thermal infrared (TIR), bands 10–14 in the 8.125 – 11.650 μm wavelength range, with 90-m resolution. The Thermal InfraRed Sensor (TIRS) is a payload of the Landsat Data Continuity Mission (LDCM) platform and acquires images using two thermal Infrared bands (10.3 - 11.3 μm and 11.5 – 12.5 μm).

For monitoring the thermal distribution in the Wuda coal field, a data acquisition request (DAR) was planned. Four DARs were submitted in 2013, which included acquisitions during days close to the spring/fall equinoxes and the summer/winter solstices. Acquisitions used the parameters: cloud coverage less than 20% and peak elevation greater than 80 degrees. As a result, four scenes were acquired successfully: two scenes on march 27 and two scenes on June 22. Daytime and nighttime pairs were available for both days. The daytime DAR in September 2013 was also successfully executed, but the observation for the winter solstice was implemented by using the TIRS sensor onboard the LDCM (Landsat 8) on December 23 instead, which have a similar spatial resolution 100 meters close to the ASTER's 90 meters. Field measurements were conducted simultaneous to satellite image acquisition. Table 1 lists scene IDs and acquisition dates and times.

Table 1. ASTER and TIRS data used in this study

Scene ID*	Acquisition date (yyyy/mm/dd)	Day/night
AST_L1B_201303272013034838	2013/03/27	Day
AST_L1B_201303272013145317	2013/03/27	Night
AST_L1B_201306222013035443	2013/06/22	Day
AST_L1B_201306222013145922	2013/06/22	Night
AST_L1B_201309262013035434	2013/09/26	Day
LC81300322013277LGN00	2013/10/04	Day
LC81300322013357LGN00	2013/12/23	Day

* Aster Scene ID is identification for ASTER images used by the Earth Remote Sensing Data Analysis Center. TIRS ID is used by the USGS EarthExplorer site. The first 12 digits of ASTER scene IDs represent the date and time of image acquisition (yymmddHHMMSS).

During field measurements, sampling blocks were used to collect land surface temperatures in the time interval between one hour before and one hour after the satellite overpass time. These data were used to estimate the accuracy of temperature retrieving and to correct for solar radiation. Samples in blocks were interpolated to high resolution (two meters) images as validation for the thresholding method. Ignition fire points observed in summer and winter were used to estimate the accuracy of the fire detection algorithm. In addition, fire boundary points identified by the field crew were recorded for comparison with the automatic fire areas delineation.

Time and topography are two key elements for accurate estimation of thermal anomalies over an heterogeneous landscape. A digital elevation model (DEM) was used for solar radiation correction, which incorporated simulated solar short wave irradiation intensity received by a unit surface area. We used ASTER level 4 data (15 m postings) as base layer due to the rapid change in topography resulting from mining and firefighting efforts. We extracted coal seam outcrop lines and boundary of the coal field from geological maps. This coal field boundary assisted in reducing our study site to an area that is able to actually cause a coal fire.

METHODOLOGY

Temperature Retrieval Methods

In this study the calibrated ASTER Level 1 B scenes were geocorrected and atmospherically corrected, resulting in upward radiance. Then the TES-MMD (Temperature Emissivity Separated, Maximum-Minimum Difference) (Gillespie et al, 1998) method for ASTER data and a split window method for LDCM TIRS data were applied to generate land surface temperature (LST) from thermal infrared data. The atmospheric correction method we adopted is part of the Thermal Atmospheric Correction module in ENVI 5.0. The method is based on the in-scene atmospheric compensation (ISAC) algorithm developed by Young et al (2002) and uses actual at-aperture radiance data in the multispectral image cube to compensate for the atmosphere and to remove the influence of up-welling and down-welling sky irradiance.

Solar Radiation Intensity Calculation

Radiative energy from the sun is mainly carried by net shortwave radiation (wavelengths from approximately 0.3 to 3.0 μm). This energy is partly absorbed and emitted as long wave radiation, which are key in climatology and environmental applications. In this study we tried to simulate this significant and probably the most thermal relevant component, net shortwave radiation S_n, which covers shortwave to near infrared, and can be expressed as:

$$S_n = (S_s + S_h + S_t) \times (1 - r) \qquad (1)$$

As in in the Equation 1, net radiation consists of radiation received by reflection of surrounding land surface (S_t), direct solar radiation (S_s) and diffuse solar radiation (S_h) modified by topography respectively. The parameter r represents the surface reflectance factor (Wilson, 2000).

For modelling topographic effects on direct radiation over a year, sun elevation and azimuth were calculated for each pixel in a DEM image as a function of latitude, solar declination angle, Julian day number, and the hour angle. Diffuse radiation affected by topography was also calculated which rely on the sky view factor in order to estimate an obstruction of overlying sky hemisphere by slope and surrounding land surfaces. Radiation received by reflection from surrounding land surfaces (S_t) can be estimated through direct and diffuse radiation using the same time unit and the terrain view factor (Böhner, 2008).

We applied the algorithm implemented as part of the SAGA GIS Lightning module.

Simulation of Temperature Increment

We proposed a relationship to explore the close connection between shortwave irradiation at sloping surfaces and bright temperature. We estimated land-surface temperature (T) by:

$$T = T_{TIR} - A \times S \qquad \textbf{(2)}$$

Where T is the land-surface temperature, we assumed that temperature retrieved from TIR images (T_{TIR}) can be calibrated by removing the solar irradiation component. A is a transformation parameter to convert shortwave radiation ratio (S) to temperature increment using dimensional K or °C.

Temperature Regression Analysis

In this study there are three sets of temperature data: (1) the LST image retrieved from the ASTER TIR and LDCM TIRS images; (2) the increment temperatures based on the DEM and the solar radiative intensity; and (3) the field measured temperature samples. We considered the field surveying temperature as the baseline and most accurate data. Considering the solar increment temperature is the correction to the TIR image inverted temperature, we used linear regression models and identified linear regression parameters. We selected the locations corresponding to the field samples as the sampling points to the TIR image and the increment images. The linear relationship is presented below:

$$T_s = T_{TIR} + A \times T_{solar} + B \qquad \textbf{(3)}$$

Where A is the gain, B is the offset, T_s is the field measured temperature samples, T_{TIR} is temperature values in the TIR temperature image, and T_{solar} are the samples in the increment image. The gain A represents the solar radiation impact on surface temperature values for a specific level and the parameter B is the bias of the simulation model for the thermal increment by solar radiation. These parameters are considered to represent the thermal correction for different typical seasons. Based on the equation of the solar altitude we can interpolated the parameters for any day of a given year.

Coal Fire Area Detection Method

The coal fire area detection method is a segmentation method with a threshold identification algorithm. Thresholds for each image self adapt to match the thermal distribution in spatial, the high gradient lines present the fire area boundary and in numerical statistics that is some auxiliary statistics parameters for prevent the false fire bondaries. For this detection method we defined prospective coal fire areas using images, which were used also for the definition of thresholds. Threshold values derive from an average temperature along the thinned lines calculated from the potential gradient buffer areas segmented with low and high thresholds to exclude the gentle and strong warming area that represent the background and fire points The buffers are ascribed as the rapid changed area from

high temperature to low temperature, which are corresponding to the fire area edge where the surface thermal attenuated in a short distance. Average mean values for potential edge lines thinned in various degrees were considered as thresholds for temperature images.

RESULTS AND DISCUSSION

Mapping Solar Radiation Simulation and Temperature

The shortwave solar radiation calculation algorithm simulated the accumulated at-an-angle solar incoming radiation (R_{ts}) and the horizontal incoming solar radiation(R_{th}). These incoming solar radiations were calculated for a time interval from one hour before to one hour after the satellite overpass time. Field-based land surface temperature measurements were simultaneous to image acquisition. Then the ratio R_{ts}/R_{th} was generated to indicate the effect of solar radiation in one pixel of the corresponding DEM image. As is shown in the fig.2 the solar short-wave radiation ratio (fig.2 (b)) was computed by the DEM. This ratio is dimensionless and reflects the increment of the temperature to a local site.

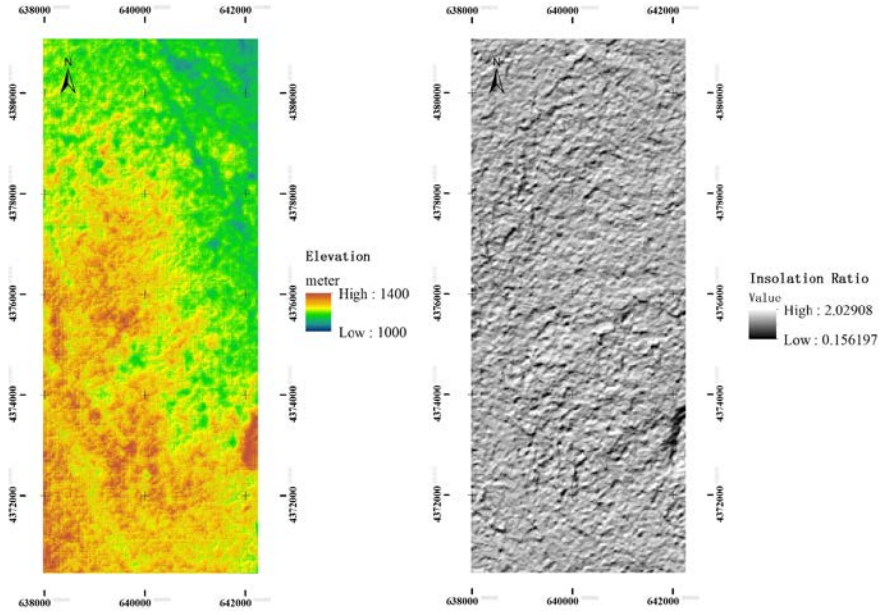

(a) (b)

Figure 2. (a) DEM and (b) temperature increment ratio calculated from the solar radiation simulation.

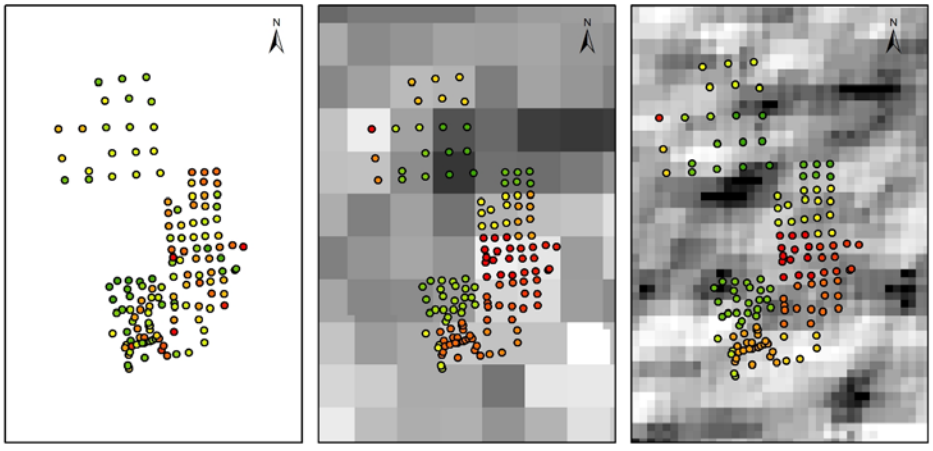

(a) (b) (c)

Figure 3. Field measured samples and corresponding temperature values and solar impact ratio values. (a) field samples for Mar. 27 2013; (b) subset of the temperature image; (c) subset of the solar radiation ratio image

Both the TES-MMD and the split window temperature retrieving methods were used to invert land surface temperature. These temperature images consist of temperature contributions by solar radiation. We used linear regression to remove solar radiation contribution by fitting solar insolation ratio to temperature difference between the samples and the corresponding temperature images.

As presented by figure 3, samples were used to extract the corresponding values from the temperature and the solar impact ratio image corresponding to the image overpass time.

Parameters for the Solar Radiation Impacts

Using temperature from field samples, associated temperature images, and the solar radiation ratio images, we estimated linear regression parameters for each of the four seasons considered. The parameters for the equation 3, $T_s = T_{TIR} + A \times T_{solar} + B$ are listed below:

Table 2. Seasonal linear regression parameters for solar radiation correction

Date	A	B
27-Mar	6.276	-17.407
22-Jun	9.1972	-17.024
26-Sep	2.4537	-3.2737
23-Dec	-2.9844	1.1901

We used these results to generate temperature images corrected for solar irradiation (fig. 3 (c)).

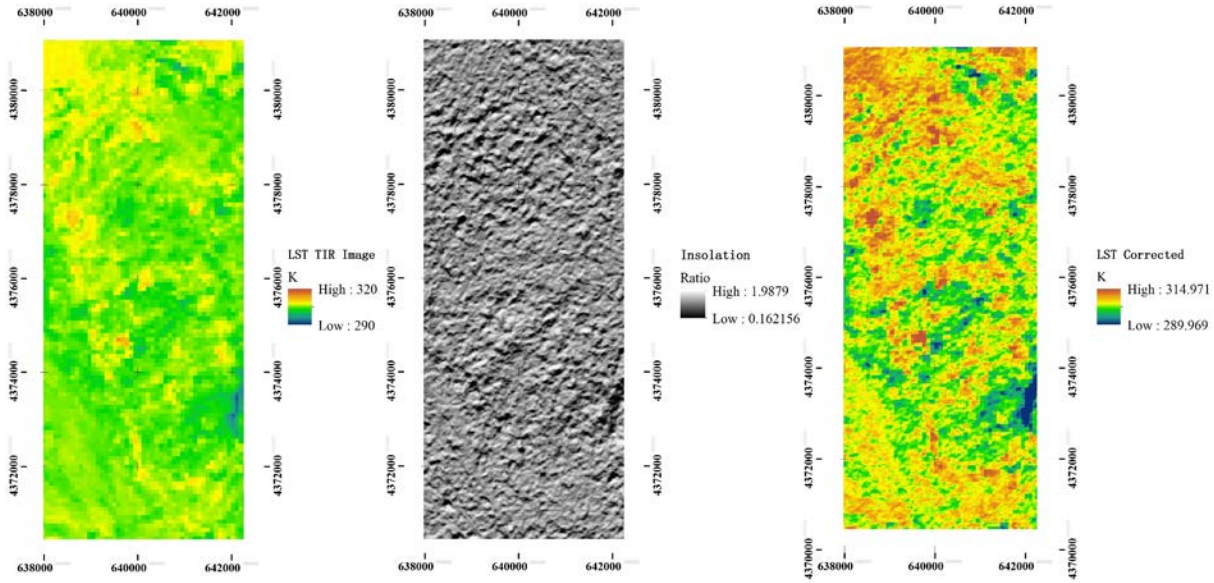

(a) (b) (c)

Figure 4. Using solar radiation intensity to correct temperatures retrieved from ASTER TIR daytime scene in Sep. 26, 2013. (a) uncorrected temperature image from TIR data; (b) solar insolation ratio image from radiation simulation; (c) corrected temperature image

Mapping Coal Fire Areas

We used the self-adaptive thresholding method to segment coal fires by temperature thresholds. We then mapped temperature anomalies, considering the coal seam outcrops and the coal field boundary. Both the original temperature image and the corrected images were used in this delineation. As shown in Fig. 4, images corrected for solar radiation result in more detailed definition of coal fires. Results are impacted by the solar radiation ratio image, which is associated with resolution improvement. The solar radiation corrected image also changed temperatures locally, impacting the definition of what pixels are tagged as coal fire.

Figure 5. Thermal anomalies from original thermal infrared images and from solar radiation corrected images for four typical seasons: March. 27 2013, June 22 2013, September 26, 2013 and December 23 2013 were mapped, listed as follows. Coal fires from original TIR imges for: (a) 2013/03/27; (b) 2013/06/22; (c)2013/ 09/26; (d) 2013/12/23; Coal fires from solar radiation corrected images for: (e)2013/ 03/27; (f)2013/ 06/22; (g) 2013/09/26;

(h) 2013/12/23; Orange areas represent coal fires; solid black lines are the outcrops of coal seams marked as coal seam number from east to west, 2,4,9,10,12

Validation Using Field Measured Boundary Points, Ignited Fire Points, and Block Samples

To investigate the accuracy of coal fire detection when using solar radiation corrected images, we mapped thermal anomalies considering field surveyed points, boundary points we traced in a fire area, and points in sampling blocks. Boundary points are points we tagged at obvious fire boundaries, such as the edge of a coal waste pile, or outcrops in the coal fire area. Figure 5 shows fire boundary points we measured on March 27 and on June 22. These points were close to the fire area or were visually identified as being on the edge of a fire area.

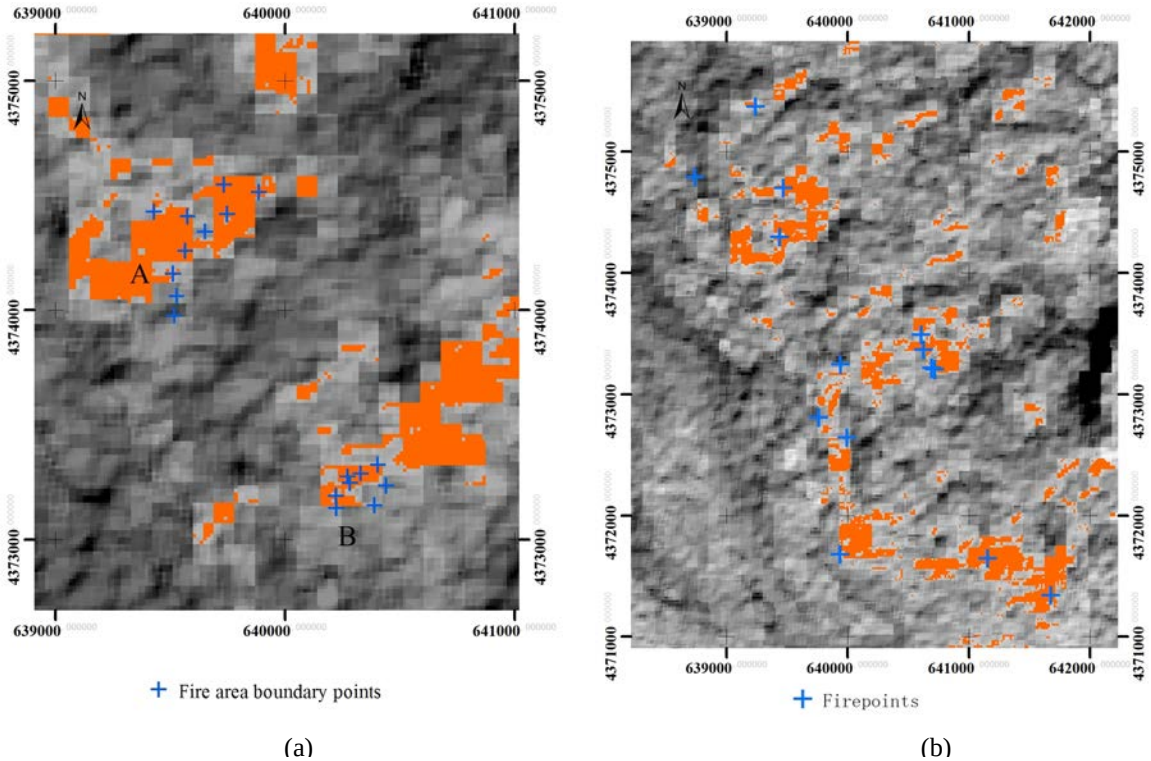

Figure 6. Thermal anomalies were limited by boundary points and by fire points. (a) coal fires for June 22, 2013 overlayed on top of fire boundary points; (b) measured fire points were compared with coal fires for March 27, 2013. These points were located near or within specific coal fires areas.

We validated our results also by using fire points measured in individual coal fire areas. We assumed that these points should locate within the retrieved coal fire area. The results are shown in Fig.6 (a) and Fig.6 (b); fire points are located inside the coal fire areas. It is not safe for us to measure fire points in the center of fire areas, including burning coal waste piles. Because of that, fire points were measured near the edge of the surveyed area. Also for this reason, shapes resulting from connecting fire points have similarities to the areas identified by our algorithm.

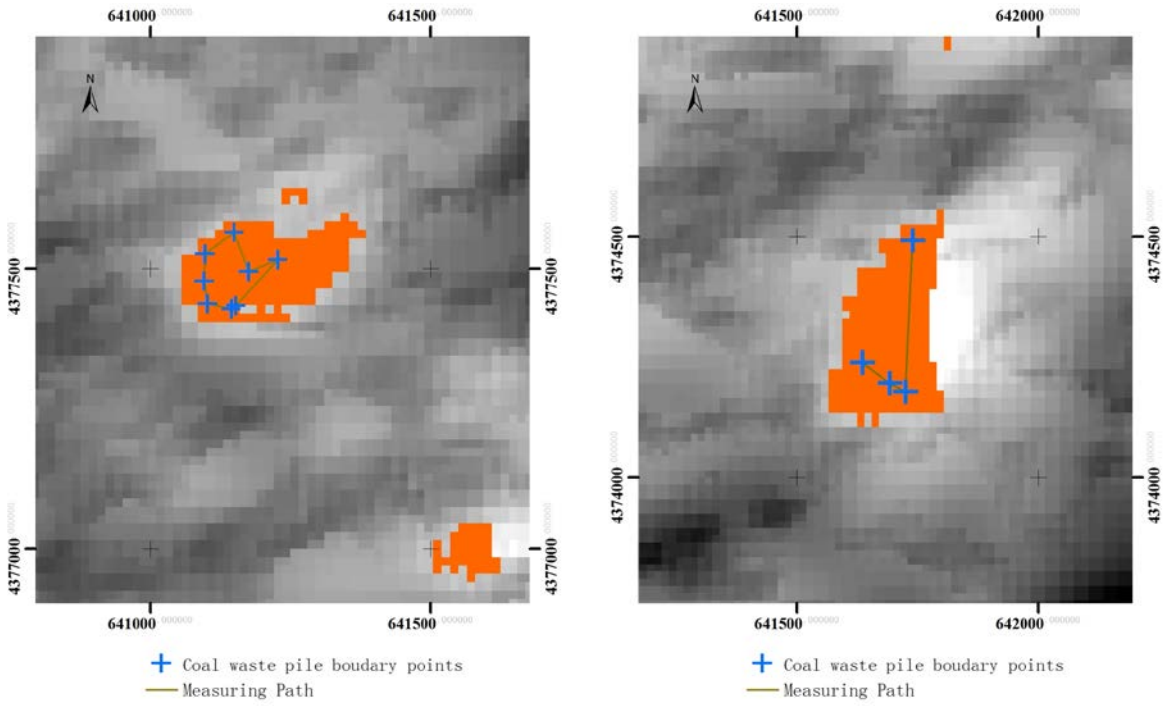

(a) (b)

Figure 7. Comparison between a thermal anomalies map and fire points. Fire points were overlaped to coal fires for Dec 23, 2013. (a) a coal waste pile area in the northern part of the coal field; (b) a coal waste pile located in the southern part of the coal field.

We used a coal fire sampling block strategy to conduct field measurements. Blocks were areas within burning coal or occupying the entire extent of the fire area. As shown in figure 7 (a), we recoded fire points for an underground coal fire area for Dec. 23, 2013. The majority of the points (84.6%) were within the detected fire area, while the outside points showed lower temperature. Points sampled in a block on March 27, 2013 were interpolated to generate a two-meter resolution temperature image. The sampling points were overlaid to this image and, as presented in Fig.7 (b), the fire areas we detected matched the high temperature areas in the interpolated image. Fig. 7 shows that the remote-sensing based fire areas fitted well the high temperature areas measured in the field. In addition, we measured coal fire points near a coal waste pile or close to a nearby road. These points were recorded adjacent to the fire areas and can be associated with the boundary of those areas.

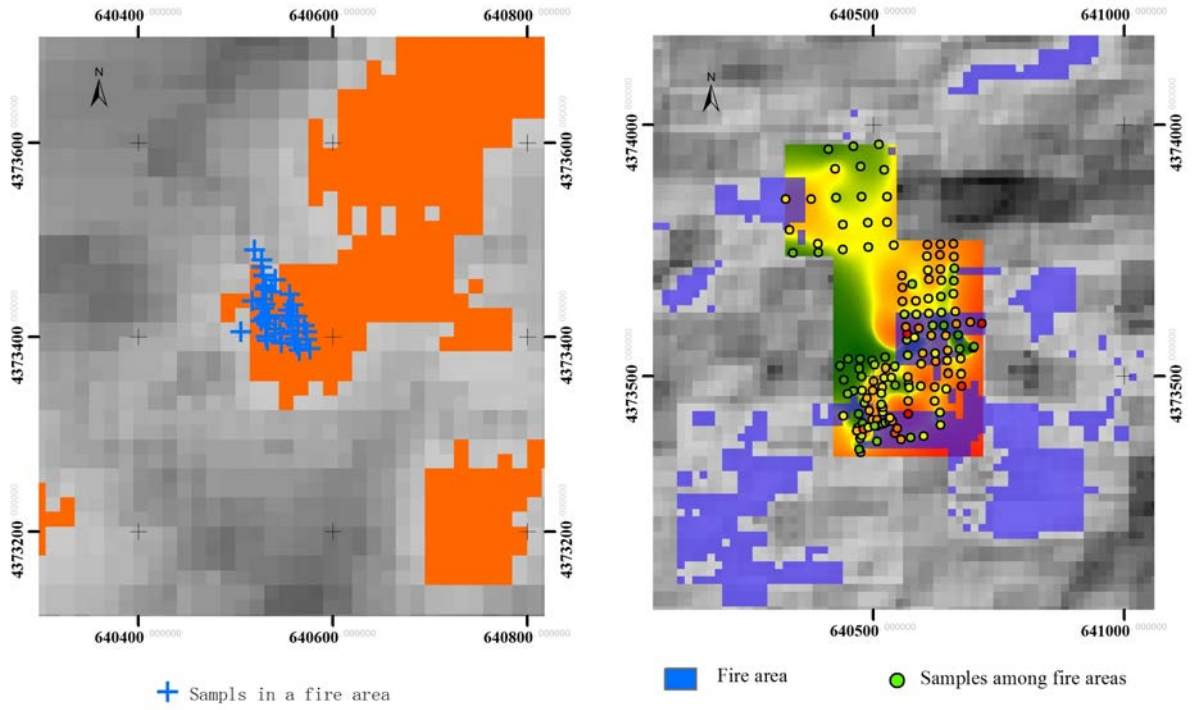

(a) (b)

Figure 8. Thermal anomalies map was compared with the sampling blocks. (a) Fire points were overlayed on coal fires for Dec 23 2013; (b) measured sampling points were interpolated into temperature images and compared with coal fires for March 27, 2013, the coal fire area (blue areas) matched the high temperature areas for field surveying.

Considering the results of both validation efforts (points, sampling traces and sampling blocks), we concluded that the detected fire area fitted well the field surveyed fire areas.

SUMMARY AND CONCLUSIONS

The TES-MMD (Temperature and Emissivity Separation-Maximum and Minimum Difference) and split window temperature retrieving methods were used to estimate coal-burning related surface temperatures in the Wuda coal field, in China. Temperature retrieval considered simulation of solar irradiance during satellite overpass for four seasons. For temperature estimation, corrections considered insolation ratio, measured land surface temperature and temperature from thermal infrared image. We reduced the solar radiation component of the TIR images to match samples collected in the field and used a linear regression approach to correct the thermal images. For coal fire detection, a self-adaptive gradient based thresholding method was used to segment thermal anomalies both for solar radiation corrected and for uncorrected temperature images. Coal fires tagged as thermal anomalies were mapped and validated by using fire edge points, fire tracing points, and sampling blocks.

We observed that coal fire areas fitted well field measured boundaries. Coal fire areas also matched high temperature areas represented by interpolated field samples. We conclude that the solar corrected images and the self-adaptive thermal images have contributed to the detection of the coal fire area. The methodology was effective in identifying fire areas for both ASTER and Landsat 8 images, with higher spatial resolution and smoother products being associated with TIRS images.

We also need to point out that the solar correction method was not applied to field measurements, and that measurements of surface temperature also were affected by solar radiation. The methodologies employed show

potential for coal fire detection and the estimation of associated attributes. Research is required to further these methodologies, including measurements of temperature underground or located in fissures.

ACKNOWLEDGMENT

This study is supported by the Strategic Priority Research Program of the Chinese Academy of Sciences (Grant No. XDA05030200). The first author's visiting study was sponsored by China Scholarship Council. The authors wish to thank the field survey team from China University of Mining and Technology. The authors also thank the faculty, staff, and students at the Center for Geospatial Research (CGR) and the Department of Geography at the University of Georgia (UGA). We particularly thank UGA's international student internship program for facilitating collaboration between the institutions involved.

REFERENCES

[1] Prakash, A., Gupta, R. P., & Saraf, A. K, 1997. A Landsat TM based comparative study of surface and subsurface fires in the Jharia coalfield, India. *International Journal of Remote Sensing*, 18(11):2463-2469.

[2] Chatterjee, R. S, 2006. Coal fire mapping from satellite thermal IR data–A case example in Jharia Coalfield, Jharkhand, India. *ISPRS journal of photogrammetry and remote sensing*, 60(2): 113-128.

[3] Zhang, J. 2008. *Underground coal fires in China: Origin, Detection, Fire-Fighting, and Prevention*. China Coal Industry Publishing House, Beijing, pp 3,383.

[4] Jiang, L., Lin, H., Ma, J., Kong, B., & Wang, Y, 2011. Potential of small-baseline SAR interferometry for monitoring land subsidence related to underground coal fires: Wuda (Northern China) case study. *Remote Sensing of Environment*, 115(2): 257-268.

[5] Kuenzer, C., Zhang, J., Li, J., Voigt, S., Mehl, H., & Wagner, W, 2007. Detecting unknown coal fires: synergy of automated coal fire risk area delineation and improved thermal anomaly extraction. *International Journal of Remote Sensing*, 28(20): 4561-4585.

[6] Kuenzer, C., Zhang, J., Tetzlaff, A., Van Dijk, P., Voigt, S., Mehl, H., & Wagner, W, 2007. Uncontrolled coal fires and their environmental impacts: Investigating two arid mining regions in north-central China. *Applied Geography*, 27(1):42-62.

[7] Wilson, J.P., Gallant, J.C. (Eds.), 2000. Terrain Analysis: Principles and Applications. Wiley, New York, pp 303.

[8] Böhner J, Antonic´ O, 2008. Land-surface parameters specific to topo-climatology. In: *Hengl T, Reuter HI (eds) Geomor- phometry: concepts, software, applications*, vol 33. Elsevier, pp 195–226

[9] Gillespie, A., Rokugawa, S., Matsunaga, T., Cothern, J. S., Hook, S., & Kahle, A. B, 1998. A temperature and emissivity separation algorithm for Advanced Spaceborne Thermal Emission and Reflection Radiometer (ASTER) images. *Geoscience and Remote Sensing, IEEE Transactions on*, 36(4):1113-1126

[10] Young, S. J., Johnson, B. R., & Hackwell, J. A, 2002. An in-scene method for atmospheric compensation of thermal hyperspectral data. *Journal of Geophysical Research*, 107(D24): 4774.